Africa Journal of Physical Sciences Vol. 8, pp. 81-102, July 2024
http://uonjournals.uonbi.ac.ke/ojs/index.php/ajps
ISSN 2313-3317

Internal Compartmentalization of the Magadi Basin, Southern Kenya Rift: Insights from Aeromagnetic and Gravity Studies

Abiud Masinde [1,a*], Aaron Waswa [1,b], George Muia [2,c]

[1]Department of Earth & Climate Science, University of Nairobi, P. O. Box 30197-00100, Nairobi, Kenya
[2]Geothermal Development Company, P.O. Box 100746-00101, Nairobi, Kenya

[a]mabiuds@gmail.com*, [b]awaswa@uonbi.ac.ke, [c]gmuia37@gmail.com

ARTICLE INFO

Article History:
Received: April 2023
Accepted: December 2023
Available online: 25 July 2024

Keywords:
Compartmentalize
Strike-Slip
Tilted Fault Blocks
Axial Zones
Flexural

ABSTRACT

The southern Kenya Rift is characterized by complex faulting and internal compartmentalization. The aim of the research is to utilize aeromagnetic and gravity data to analyze compartmentalization, sediment thickness, and structural characterization. Using tilt derivatives, regional-residual separation, and Euler solutions allow for separating important structures, and lineaments. Euler solutions determine the depths and positions of causative sources. Unconstrained 3D susceptibility model reflects the compartments and surrounding geological formations. Compartmentalized structures are observed across three grabens, each with unique geological features and fault orientations. The first western graben displays tilted fault blocks and z-shaped depocenters, suggesting a strike-slip strain regime. Significant shifts in rifting style have influenced fault activity and strain concentration mechanisms. The Aswa-Nandi-Loita transfer zone greatly influences compartmentalization, fault structures, and sedimentary deposition. Analysis of sediment thickness reveals deeper signatures in the first graben that domiciles Musenke [2700m], Pakase [2600m], and Olkiramatian [1700m], depocenters. These variations are attributed to boundary fault constraints and volcanic manifestations influencing sedimentation patterns. The second graben exhibits thinner sedimentary compartments encompassing Magadi, Kordija, and Mile Forty-six. Structural characterization reveals rotated fault blocks dominating the first graben, axial zones characterized by E-W and NE-SW linear orthogonal structures in the second graben, and flexural regimes in the third graben.

1. Introduction

As Kenya's petroleum exploration efforts increase, all known sedimentary basins become the subject of extensive research. Growing needs for discoveries have forced the expansion of exploration activities into volcanic terranes. This research concentrates on Kenya's Magadi basin within the southern Kenya Rift system [Fig. 1], where flood basalts mask sediments targeted for petroleum exploration [1]. The Kenya Rift System comprises numerous sedimentary basins, such as Turkana, Lotikipi, Lokichar, Kerio, Magadi, and Baringo. These rift systems have been

extensively studied through various surveys, encompassing 2D and 3D seismic surveys and FTG (Full Tensor Gravity), gravity, and magnetic surveys. Exploration efforts in northern Kenya have predominantly concentrated on the rift basins, leading to the drilling of more than 40 exploration and appraisal wells. The Magadi sedimentary basin constitutes the southbound part of the Rift Network in Kenya and has received limited exploration attention due to its complex geology [Fig. 1]. The Rift Network in Kenya is distinguished through its extensive volcano-tectonic activity traced back to the Paleogene era [2]. The complexities arise from the multiple volcanic episodes that have shaped the evolutionary history of the Magadi basin [3]. These volcano-tectonic complexities are responsible for the internal compartmentalization of the Magadi basin [2]. Comprehending these compartments' location, architecture, structural evolution, and tectonics is vital in hydrocarbon prospecting.

Studies conducted on the potential reservoirs and source rocks around the Nguruman escarpment and river Entasopia revealed good reservoir sandstones that are not susceptible to diagenesis. The shales and mudstones are possible mature source rocks, sufficiently buried since the area has a high geothermal gradient evidenced by the hot springs around the lake [2]. The green bed formation has been established to contain organic-rich mud. They are lacustrine shales of Type 1 /II Kerogen [algae source] with good organic richness [TOC= 3.28%]. They are relatively young, first dated at around I Ka [Pleistocene], and offer a foundation for hypothesizing that comparable carbon-based rich beds might have formed in prior paleo-lakes. The algae forming at Lake Magadi can be related to the mudstone outcropping on the shores of River Entasopia. The Magadi Transverse Zone, a strike-slip fault, has substantial inferences regarding the hydrocarbon trapping system and migration. Based on the sealing basalt formation, shale formation as the source rock, and the sandstone formation as the reservoir unit, a functioning petroleum system might exist in the depocentres of Musenke, Olkiramatian and Pakasee.

Oil and gas reserves have been discovered in similar basins in China, such as Bohai Bay, Songliao, and Junggar. These basins contain Cenozoic basalts that were primarily formed in subaerial surroundings, with a total thickness exceeding 1000 meters [4].

The research employed various methodologies, encompassing Euler deconvolution of aeromagnetic data, application of Butterworth low-pass filters to aeromagnetic data, and gravity gradients. It is noteworthy that magnetic signatures within sedimentary formations exhibit considerably lower values compared to metamorphic and igneous formations, leading to notable petrophysical variances [5]. Consequently, aeromagnetic data methods are employed to discern major volcanic and basement systems within the southern Kenya Rift system [6, 7].
Prior investigations in the Kenya Rift aimed to enhance understanding of seismic activity and crustal structures. Studies by [8-11] employed seismic profile data to scrutinize the crustal features beneath Kenya's Rift System. [12, 13], identified crustal extensional stress fields within the central Kenya Rift by integrating well logging data, passive seismicity earthquake information, and field data. [14] comprehensively analyzed upper crustal structures, utilizing geological, gravity, well logs, and seismic profiles. [15] demonstrated the structural setting of the upper

mantle using seismic profiles, while [16] investigated seismic activity in the southern Kenya Rift. [17] discovered basalt sequences interbedded with chert and clay in borehole cuttings from Lake Magadi. [18] utilized aeromagnetic data to explore deep-seated faults and determine the Curie-point depth. [19] identified a Jurassic-aged palaeo-triple junction in southeastern Kenya through aeromagnetic data analysis. [20] adopted a multi-physics methodology, incorporating electrical resistivity, aeromagnetic data, and ground magnetic traverses to examine fault network characteristics.

Despite the importance of compartmentalization due to the volcano-tectonic process, little work has been done to understand these compartments for hydrocarbon prospecting. This research reveals the evolution, architecture, sediment thickness, sediment quality, and the volcano-tectonic complexities of the compartments in the Magadi basin. The study maps out these compartments and reveals each compartment's suitability for hydrocarbon exploration.

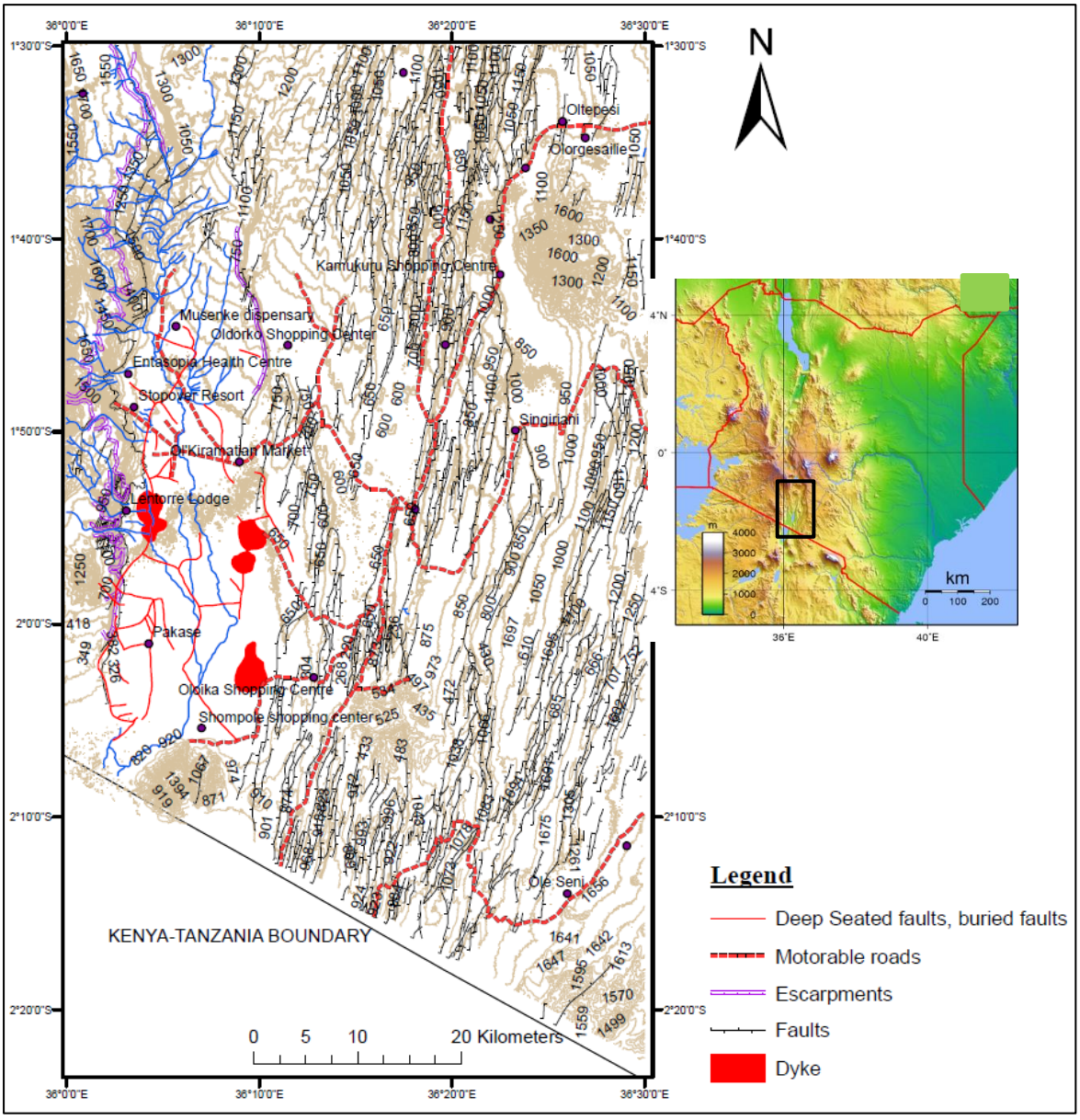

Figure 1: A map of the research location with structural details [modified from [1]]

2. Geological and tectonic setting

The East African Rift System [EARS], characterized by extension tectonics, extends from the Red Sea to Mozambique [22-25]. It comprises three primary rift basins in the southern, northern, and central regions [22]. These extensive sedimentary systems are equally sub-divided into minor sedimentary systems characterized by closely spread out normal faulting of Quaternary age [26, 27]. The Magadi area's vicinity exhibits distinctive geological features, including metamorphic and volcanic systems dating back to the Precambrian, as well as sedimentary rocks from the Holocene era [Fig. 2] [1, 28]. Notably, the Nguruman escarpment provides visible outcrops of Precambrian metamorphic rocks in western areas of the Southern Kenya Rift[Fig. 2]. A Precambrian metamorphic system underlies the olivine basalts that erupted 3.1 to 2.5 million years ago (Piacenzian-Gelasian) [29]. The Kirikiti platform is mainly composed of olivine basalts and is located on the fault scarp near the Nguruman escarpment [30].

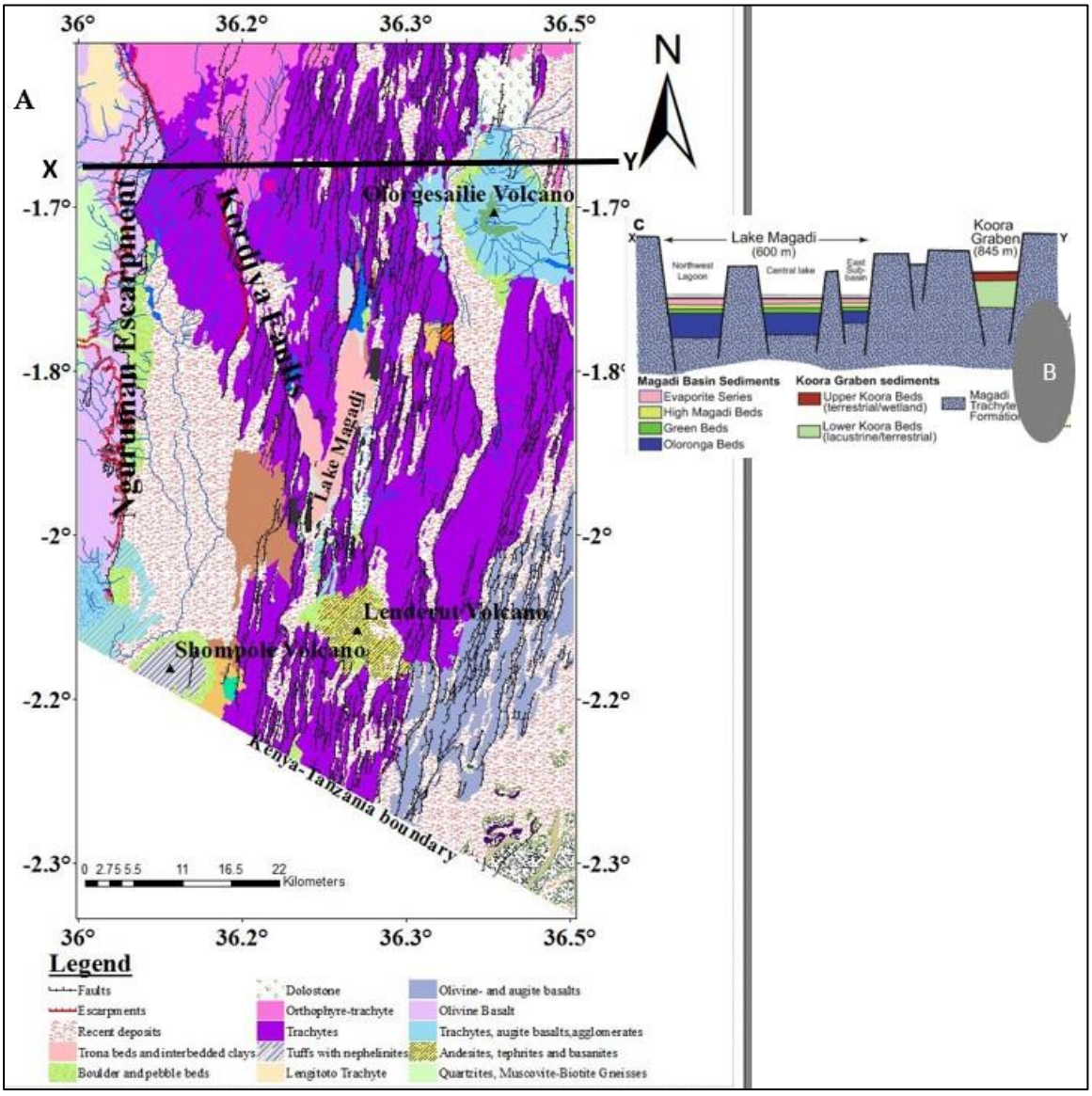

Figure 2: [A] Geological setup of the Magadi Basin while [B] is the geological cross-section across the Magadi area after Renaut and Owen [31]

The basin's stratigraphic sequence comprises fluvial, lacustrine, and volcanic units, each presenting distinct hydrocarbon potential. The lower stratigraphic units, characterized by coarse-grained fluvial and alluvial fan deposits, may serve as potential reservoirs due to their porosity and permeability. Overlying these are fine-grained lacustrine deposits, including mudstones and siltstones, which can act as effective source rocks if they contain sufficient organic material and have experienced appropriate thermal maturation. The intermittent volcanic activity recorded in the basin's stratigraphy, through ash layers and lava flows, may contribute to structural traps and seals necessary for hydrocarbon accumulation. Moreover, the evaporitic sequences, particularly those rich in trona and halite, might indicate periods of restricted basinal conditions conducive to organic preservation.

The region's faults may be classified into three categories: tiny intra-rift faults directed N-S and larger rift-bounding faults oriented NNE-SSW, NNW-SSE, and large N-S [32, 33]. The interaction between fault evolution, volcanic activities, and volcanic episodes has created several basins with unique shapes influenced by tectonic forces [34]. Sedimentary deposits from previous high lake occurrences are found in the basins, combined with and located above the core volcanic structures [34-36]. Aside from the Rift and its associated volcanic episodes, other important geological manifestations exist. The western area contains the Tanzania craton, which is of Archaean age and consists of exposed granitoid gneisses and metavolcanic. The Aswa-Nandi-Loita (ANL) shear zone is oriented in a NNW-SSE to NW-SE direction and marks the northeastern edge of the craton [37]. The geophysical results show that the area where the Oloololo escarpment meets Lake Magadi is the southerly boundary of the craton in Kenya [38]. The pre-existing framework has influenced the architecture and positioning of the Kenya Rift in the south. The existing structure triggered and reactivated the Aswa-Nandi-Loita (ANL) shear zone [39]. The southern Kenya rift was created on a significant cratonic lithosphere [40]. Rocks from the Mozambique belt are thought to have been uplifted above a modified craton, extending about 100 km towards the eastern border between the belt and the craton [41]. The reworked craton margin stretches in a northwest-southeast direction and is defined by the Aswa-Nandi-Loita shear system at its northern edge. The Southern Rift in Kenya is a volcanic-dominated basin, 50 to 70 km wide, bordered by notable normal faults [42].

The tectonic-magmatic development of the Southern Kenya Rift is often divided into two phases. Several lava flow patterns dominated with unique spatial distribution during the initial period (7 – 1.3 Ma)(Messinian-Calabrian). The Longitoto trachytes, about 7 million years old (Messinian), began to deposit during the first phase of the Magadi-Natron rift depression [Fig. 2]. After the first flood lavas, axial shield volcanoes emerged, such as Olorgesailie (2.7 to 1.7 Ma)(Piacenzian-Calabrian, Lenderut volcanoes, and Shompole volcanoes (2.0 Ma)(Gelasian) [42-44]. Magmatism commenced after that, during the outpouring of basaltic floods 3.5 ma (Piacenzian) [32]. Between 1.3 million years ago (Calabrian) and the present, another episode of flood-type lavas resulted in the eruption of Magadi trachytes dated 1.3 and 0.9 Ma (Calabrian) over the Magadi-Natron area, which was experiencing significant subsidence. The eruption coincided with substantial fault movement along the western border fault [32, 45]. During the subsequent rifting phase, a

notable change occurred with the formation of a series of normal faults aligned along the Rift, leading to disturbance in the inner base of the Magadi trachyte [32, 45, 46]. The transmission of strain down the rift axis is believed to have occurred due to the discharge of magma and related materials [47]. The Kordjya fault line demonstrates how the local structural arrangement of the basement affects the morphology and movement of intra-rift networks.

Fig. 2 shows the surface geology of the Magadi area, which is composed mainly of metamorphic rocks from the Precambrian, volcanic rocks of the Plio-Pleistocene, and Holocene–Recent Period sedimentary deposits [3]. Metamorphic rocks from the Precambrian era may be seen in the exposures at the Nguruman escarpment along the Nguruman border fault [48]. Multiple volcanic formations are present in the Magadi region, with Olorgesailie as the most pronounced. The Olorgesailie volcano, which formed 2.7 Ma (Piacenzian), consists of a varied mixture of olivine basalts, nephelinites, and alkali trachyte. With an estimated 2.5 million years(Gelasian), the Lenderut volcano [Fig. 2] in the southern area displays a range of magmatic flows ranging from basalt to andesite. Carbonatite and nephelinite minerals comprise the Shompole plug [Fig. 1], which erupted 2 Ma (Gelasian) [22]. Quaternary sediments accumulated in the Magadi basin [3, 48]. Underneath Lake Magadi are sedimentary and volcanic deposits that date from the Miocene to the Pliocene [3, 32, 48]. A similar subterranean sedimentation is expected to have occurred about 7 Ma in the Late Miocene, concurrent with the Nguruman fault's development. Recent formations in the Magadi area are typically sediments of lacustrine and fluvial origins [49, 50].

3. Data, Methods, and Analysis

3.1 Aeromagnetic Data analysis

The Compagnie Generale de Geophysique [CGG] collected the aeromagnetic data used in 1987. This airborne magnetic data collection aimed to support the African Magnetic Mapping Project (AMMP) by collecting data from several African sites. The survey covered an overall distance of 148 km, which was executed utilizing east-west flight lines separated at 2 km using a highly sensitive cesium vapor magnetometer. The average total area of the 241 flight lines was 482 km × 148 km. The altitude variations compensation factor was 0.025 nT/meter, based on barometer altitude [35]. The dataset obtained at the ground base station were deducted from the synchronous in-flight observations at intervals of 0.5 seconds to account for diurnal variation. The residual values were adjusted by adding the constant computed mean magnetic value of 33,650.49nT. The IGRF 1987 formula determined the regional field at 9500 feet in height at half-second intervals along the profiles [35].

The residual magnetic readings at the intersection of the lines and the tie lines were compared to examine the leveling errors. At each intersection, the difference between the residual values of the line and tie lines is determined by extrapolating the reductions made near line crossings. Datasets corrected for leveling errors were gridded via the bicubic spline approach. Readings were then adjusted to account for variations in elevation by compensating with a

0.025nT/meter factor. The barometric elevation was utilized to calculate this altitude correction. The results were subsequently re-projected to the WGS 84-UTM 37S, equivalent to one kilometer above the surface level projection used in this study [35].

To generate symmetrical anomalies centered around their respective causal structures, the TMI anomalies were reduced to pole [TMI-RTP] by the 2019 MAGMAP algorithms of Sequent. Inclination and declination values linked to the Magadi location are about -26.2° and 0.003°, respectively are utilized. All subsequent derivatives were calculated using the RTP grid as the principal input grid.

3.2 Gravity Data analysis

The methodology employed in this study involved the analysis of gravity data collected through 530 ground-based measurements over a 281-square-kilometer region [Fig. 3]. Spaced at intervals of 500 meters by 3 kilometers, these measurements were used to generate the Simple Bouguer Anomaly map (SBA) using a uniform density of 2.67 g/cm^3. The minimal curvature algorithm was applied to enhance spatial resolution, resulting in the gridding of the SBA with a resolution of 100 meters.

The derived Simple Bouguer Anomalies effectively capture the gravity variations within the surveyed region. Notably, the map reveals a discernible and consistent increase in gravity signals from the northern to the southern areas. Additionally, a detailed map analysis unveiled distinct characteristics, where deep sources exhibited continuous long-wavelength signatures over extensive regions, while shallow features generated sharp signatures characterized by short wavelengths.

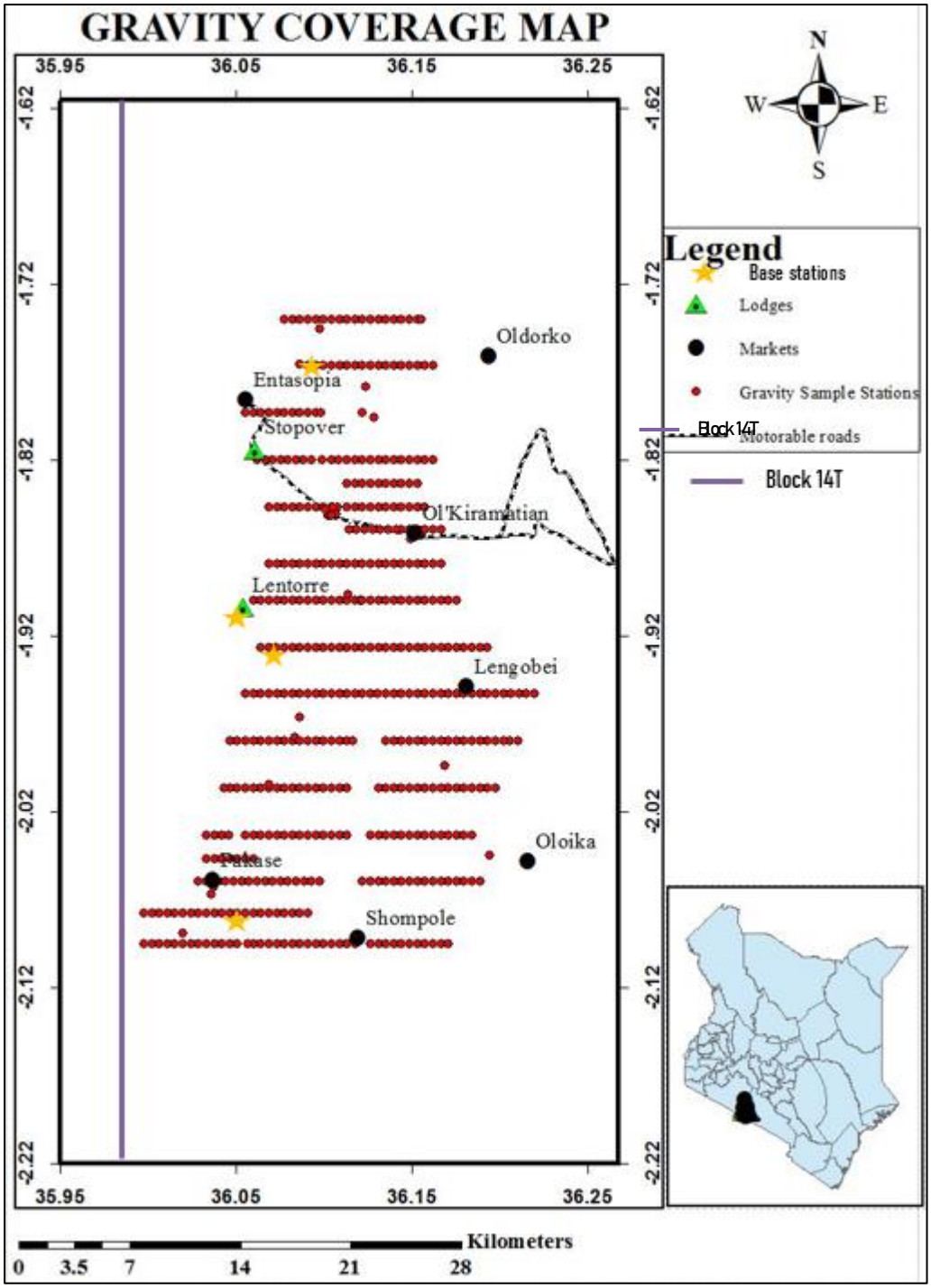

Figure 3: East-West oriented acquisition lines for the gravity survey

3.3 Regional versus residual gravity and magnetic anomaly separation

Upward continuation is a filtering technique in Oasis Montaj that utilizes mathematical analysis to transfer the gravity field onto a plane positioned above the survey datum plane, creating geological anomalies. One may use mathematical techniques to project a Bouguer gravity map over a predetermined reference plane to provide a smoothing effect. The influence of residual anomalies caused by gravity decreases as the height of the projection increases since the effects

of regional anomalies become more significant [51]. The algorithmic implementation of upward continuation in Oasis Montaj involves coding the equation [Eq.1]

$$L(\omega) = e^{-h\omega} \quad [1]$$

Where $L(\omega)$ represent the log of angular wavenumber, e is the exponential component, and h denotes the vertical distance above the viewing plane. The Bouguer anomaly grid was extrapolated to a distance of 50m to estimate the suitable height for upward continuation. As the distance of continuation diminishes, the impact of shallow, tiny, and isolated geological features becomes more pronounced [Fig. 4a].

3.4 Euler Deconvolution method (ED)

The Euler deconvolution technique was utilized to identify the positions of structural lineaments and approximate depths to the top of magnetic causatives in the investigated area. This method is favored as it does not depend on prior knowledge of the magnetization direction of the causatives, and the results obtained are not influenced by any remanence degree [52]. [53] created a computerized technique for examining data along magnetic profiles. [54] enhanced the gridding magnetic profile data technique. Several authors have utilized Euler Deconvolution [ED] to estimate the apparent depth of causative sources in aeromagnetic data analysis [55-59]. This method addresses data gradients, effectively tracking contacts and determining depth estimates to causative bodies. Given that ED is a solution-based method, the anticipated contacts are close to the source locations in areas with homogeneity in susceptibilities. Due to this, Euler analysis relies on magnetic data derivatives. An essential use of fast Fourier transform is to find the initial vertical gradient of magnetic data [60]. The Fast Fourier Transformation (FFT) technique is utilized to compute derivatives in the horizontal (HDR) and vertical (VDR) orientations based on the initial vertical gradient. Trends in structure and lithology are defined by using causal bodies in the horizontal orientation obtained from Euler's calculations. The source lies where solutions tend to cluster together.

This study considers that magnetic interactions identify source edges and delineate sedimentary basins. When considering Euler deconvolution, the window choice and Structural Index [SI] are two widely recognized parameters. This method identifies the source of the causal body by presuming that the type of the geo-body is defined by a conventional Structural Index [SI]. The studies by [53, 54] demonstrated that the optimal structural index resulted in the most accurate clusters of solutions. A window size of 32km by 32km is employed to represent the influence of the boundaries of causative structures. Euler's homogeneity equation determines the apparent depth of causative sources [60-62]. The clustered solutions were determined with SI = 0 and a 10% margin of error.

3.5 Tilt derivative (TDR) method

This study uses the TDR edge detection technique to map the main faults and related geological features in the Magadi area. The TDR approach was initially suggested by [63] and formalized by

[64]. TDR is the arctangent of the ratio between HDR and VDR, where HDR denotes the sum of all horizontal derivatives, and VDR signifies the vertical derivatives. Regardless of the magnitude of the VDR or HDR, the amplitudes of the derivative of the tilt angle range from -90 degrees to +90 degrees [65]. TDR becomes inclination-dependent at 2D magnetic source body edges such as faults, dikes, and blocks but crosses zero at 0° and 90°. On the other hand, the source is horizontally positioned at the measurement point (x = x0) beyond the contact limits, where the tilt angle is zero degrees. To locate thrust and fault zones, some researchers have used tilt derivative investigations [63, 66-71].

3.6 Three Dimensional Magnetic Inversion

In the last 20 years, voxel-based modeling and inversion have become widely used methods in geophysics. Revolutionizing the way geophysical data, such as gravity and magnetics, are inverted into three-dimensional models using Oasis Montaj's geophysical software module, VOXI Earth ModelingTM. A CaRTPsian Cut Cell (CCC) inversion technique is used in the approach, as proposed by [72]. More recent work by [73] has improved the algorithm's ability to describe geological surfaces accurately. [74] shows that Inversions may be executed without constraints.

Several inversion methods are available [72, 74-76]. The model's sensitivity was refined by making iterative adjustments to maximize the data fitting process and reduce the average gap between the model's projected values and the actual observed data. Several fitting methods were investigated, such as absolute and relative errors, as well as the standard deviation fraction [77-80]. The aeromagnetic data from the Magadi area was used to create a three-dimensional inversion model. With a total coverage of 7209 km2, the model comprises 38 grid cells along the horizontal axis and 46 grid cells along the y-dimension. On the horizontal axis, this measurement translates to 81 km, while on the y dimension, it is 89 km. The model's six vertical grid blocks extend 10 kilometers below Earth's surface. The anticipated reduction in vertical resolution was accommodated by allowing the thickness of vertical cells to rise gradually with depth. The data was pre-processed by subtracting a linear baseline before inversion. The VOXI setup developed by Oasis Montaj produced a 1 nT magnetic data correlation. If the data are not constrained, the susceptibility distribution is uniform. A detailed three-dimensional model is generated, reflecting the sub-basins and surrounding geological formations, as deduced from the unconstrained models. To confirm the models, comparisons were made between the values observed in the survey samples and the outcomes of other related studies.

4. Results and Discussion

4.1 Compartmentalization of the southern Kenya rift

The southern parts of the Kenya Rift system are highly faulted and segmented, as shown on the residual maps [Fig. 4]. From aeromagnetic anomalies [Fig. 4a], the Magadi area can be broadly classified into two: - the high magnetic areas with values ranging from 13nT-70nT associated with volcanic or basement sources and dominant low magnetic areas with values ranging -12nT—

437nT associated with sedimentary signatures in the basin. These compartmentalized signatures imply different strain regimes within the southern Kenya Rift.

The sedimentary signatures are disturbed across the basin along the three grabens. The first graben [G1] is the initial graben that is near the main boundary fault on the west and constitutes the Pakase [PK], Olkiramatian [OK], and Musenke [MU] depocenters. Faulting within the first graben [G1] is constrained by the boundary fault to the west and the volcanic horst to the right. SBA residual anomalies [Fig. 4b] depict three main structural trends: a prominent set moving in the N-S direction, a moderate set running in the NNE-SSW direction, and a minor set trending in the NNW-SSE direction. The first graben is dominated by tilted fault blocks and the z-shaped depocenters pointing towards a strike-slip strain in areas closer to the boundary fault. Studies by [81] point out significant shifts in the rifting style observed during the more recent stage of rifting (1.3 Ma-Present). These changes led to a concentration of strain through two main mechanisms: i) the movement of fault activity from the Ol Doinyo Ogol Fault to the Sambu-Natron fault as well as from the west to the east Nguruman fault in an eastward direction, and ii) the occurrence of faulting within the Rift itself, which initially accommodated a portion of the extension in the Magadi-Natron trough [81].

A volcanic horst separates the first graben [G1] from the second graben [G2]. The sedimentary compartments within the second graben [G2] include Magadi [MD], Kordija [KD], and Suswa [SU] lie on the east of the Aswa-Nandi-Loita [ANL] transfer zone. Aswa-Nandi-Loita [ANL] corridor exhibits fault boundaries and is characterized by en-echelon small-scale graben and horst structures [Fig. 4b]. The structures take on Z-and S-shaped forms with their terminations parallel to the western border fault [Fig. 4b]. The structures exhibit trans-extension due to inherited heterogeneities in the oblique substratum. Musenke, Pakase, Olkiramatian, Koora, and Forty-six depocenters have been formed by the segmentation and compartmentalization of subsurface rocks along NW–SE shear faults. The Aswa Nandi Loita [ANL] transfer area is a strike-slip fault spanning NW-SE, the most recent fault in the basement [20]. Kenya's Rift system has the most upper crustal extension due to the brittle strain in the Magadi section. Most of this extension (89-82%) is attributed mainly to displacements along the fault network that bounds the Rift. Based on the limited extent of extension related to faults within the Rift, inner faulting is not the primary method for accommodating the strain in the Southern Kenya Rift throughout the inward strain. Furthermore, there is no sudden shift from strain accommodation dominated by border faults to strain accommodation dominated by faults within the Rift over time, as is commonly observed in young rift segments [81]. The third graben [G3] is localized in the eastern parts of the basin, with the Koora sub-basin as the dominant depocenter. A 3D separation of susceptibilities confirms the existence of a compartmentalized basin [Fig. 5]. The fragmentation of the Southern Kenya rift system seems to have been linked to the volcanoes identified by the 3D aeromagnetic model [Fig. 5] in the study region. Compared to the other grabens, sedimentary compartments within the first graben [G1] in the western regions are heavily influenced by near-surface volcanic flows. Gravity SBA residual results [Fig. 4b] unmask the hidden sedimentary compartments and reveal

the architecture of these compartments. Near-surface volcanism concealed these compartments on the TMI-RTP-residual results [Fig. 4a].

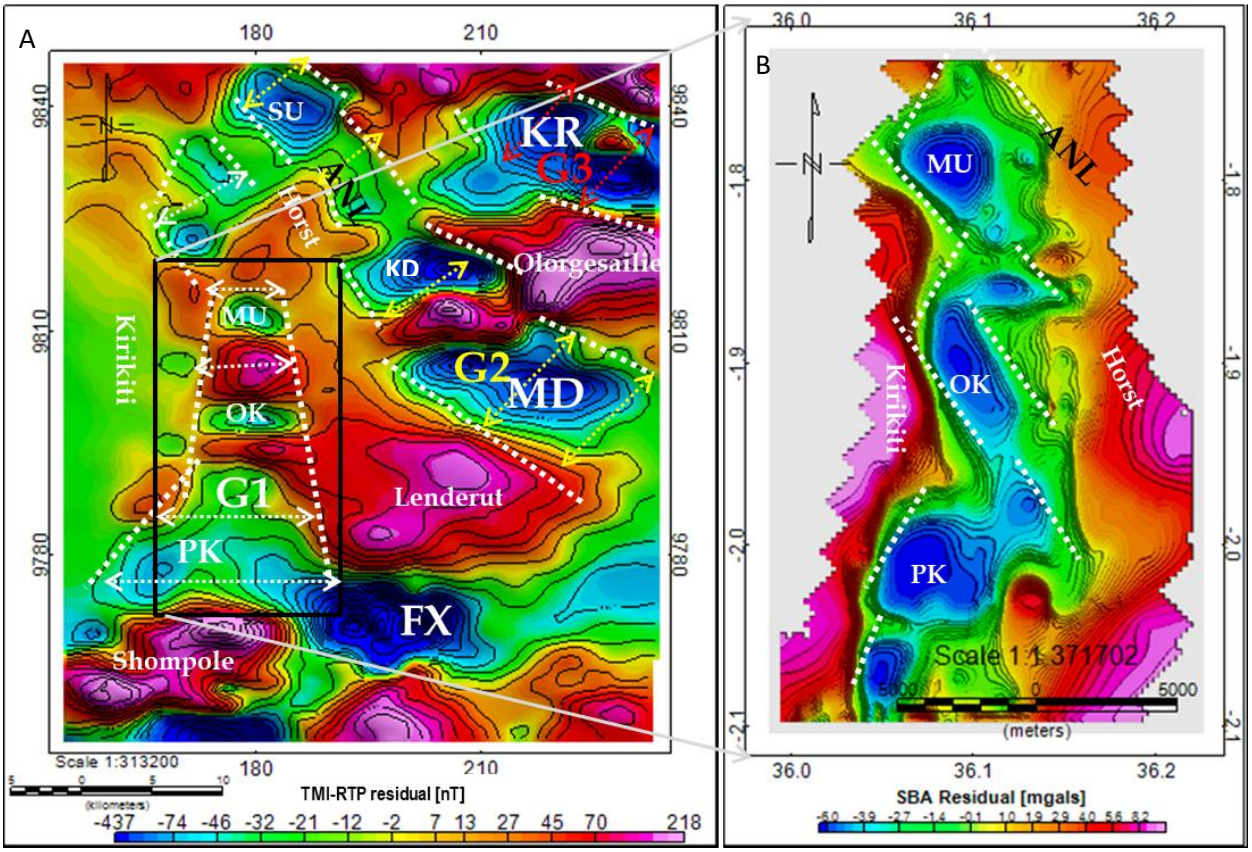

Figure 4: [A] is the TMI-residual map derived from aeromagnetic data while [B] is the SBA residual anomalies delineating the depocenters in the first graben

TMI-residual map figure 4 [A] derived from aeromagnetic data delineates the three grabens, depocenters, and volcanic plugs. The area highlighted in black shows the location of gravity data. On the map; G1=first graben, G2=second graben, G3= third graben, SU=Suswa, KR=Koora, KD=Kordija, MD=Magadi, MU=Musenke, OK=Olkiramatian, PK=Pakase, FX=Mile Forty-six, and ANL=Aswa-Nandi-Loita. The SBA residual anomalies figure 4 [B] delineates the depocenters in the first graben, where, MU=Musenke, OK=Olkiramatian, and PK=Pakase.

One of the implications of the intense compartmentalization on the hydrocarbon prospects is the isolation of source and reservoir rocks from the dominant volcano-sediments. Therefore, source and reservoir rocks from the compartmentalized sections of the basin have higher quality compared to the one from non-compartmentalized sections.

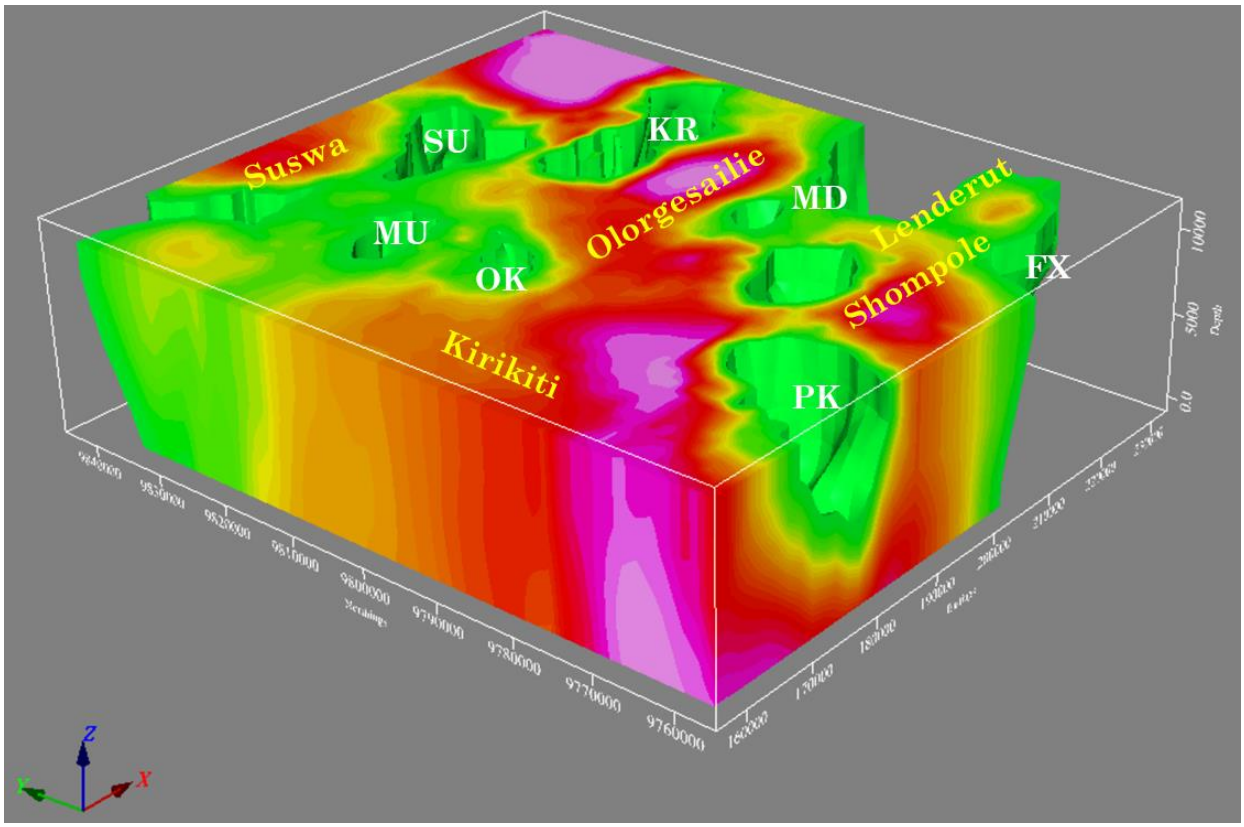

Figure 5: Unconstrained three-dimensional aeromagnetic susceptibility model showing the compartments

The unconstrained three-dimensional aeromagnetic susceptibility model in figure 5 shows the compartments and surrounding geological formations, where, SU=Suswa, KR=Koora, KD=Kordija, MD=Magadi, MU=Musenke, OK=Olkiramatian, PK=Pakase, FX=Mile Forty-six.

4.2 Analysis of sediment thickness

Results from Euler Deconvolution [Fig. 4] and 3D aeromagnetic modeling [Fig. 5] have been utilized to approximate the depth and thickness of the different sedimentary compartments in the Southern Kenya Rift and tabulated [Table 1]. Sedimentary compartments within the first compartment [G1] show deeper signatures than the rest. For the Musenke depocenter [MU] within the northern parts of the first graben [G1], the aeromagnetic signature ranges from -2nT to -437nT while SBA anomaly signatures range from -1mgals to -6mgals [Fig. 4]. Depths estimates from Euler solutions [Fig. 6] and verified by the 3D susceptibility model [Fig. 5] vary between 1600 and 4300 meters spanning over 12sq kilometers. The NW-SE oriented boundary fault constrains sedimentation, and the sequences dip towards the north. Olkiramatian Depocenter [OL] equally dips towards the north and is bounded by the NW-SE oriented boundary fault [Fig. 4]. A horst on the eastern section constrains sedimentation towards the east [Fig. 4]. Results from the residual analysis [Fig. 4] exhibit a range of -2nT to -88nT for aeromagnetic signatures, while the SBA anomaly signatures span from -1mgals to -5mgals. The estimated depths obtained using Euler solutions [Fig. 6] and then validated by a 3D susceptibility model [Fig. 5] show a range of 1800 to 3500 meters covering over 15sq kilometers.

Pakase depocenter [PK] forms the southernmost compartment of the first graben [G1] [Fig. 4]. Pakase depocenter [PK] has a northward dip delineated by the boundary fault oriented in a NE-SW direction [Fig. 4]. The volcanic manifestation associated with the eastern Lenderut constrains the sedimentation towards the east [Fig. 4]. The residual analysis results [Fig. 4] show that aeromagnetic signatures vary from -1nT to -98nT, while the SBA anomaly signatures range from -1mgals to -6mgals. The depth estimates made from Euler solutions [Fig. 6] and then confirmed by a 3D susceptibility model [Fig. 5] show a range of 1600 meters to 4200 meters, which covers more than 30 square kilometers. The three depocenters within the first graben portray an average sediment thickness of about 2400m. Studies by [44] approximate the western grabens depth of 6 km, encompassing the volcanic and sedimentary sequences. Extension within the Magadi half-graben over its 7 million-year-long (Messinian) rift evolution has been described in studies conducted by [81].

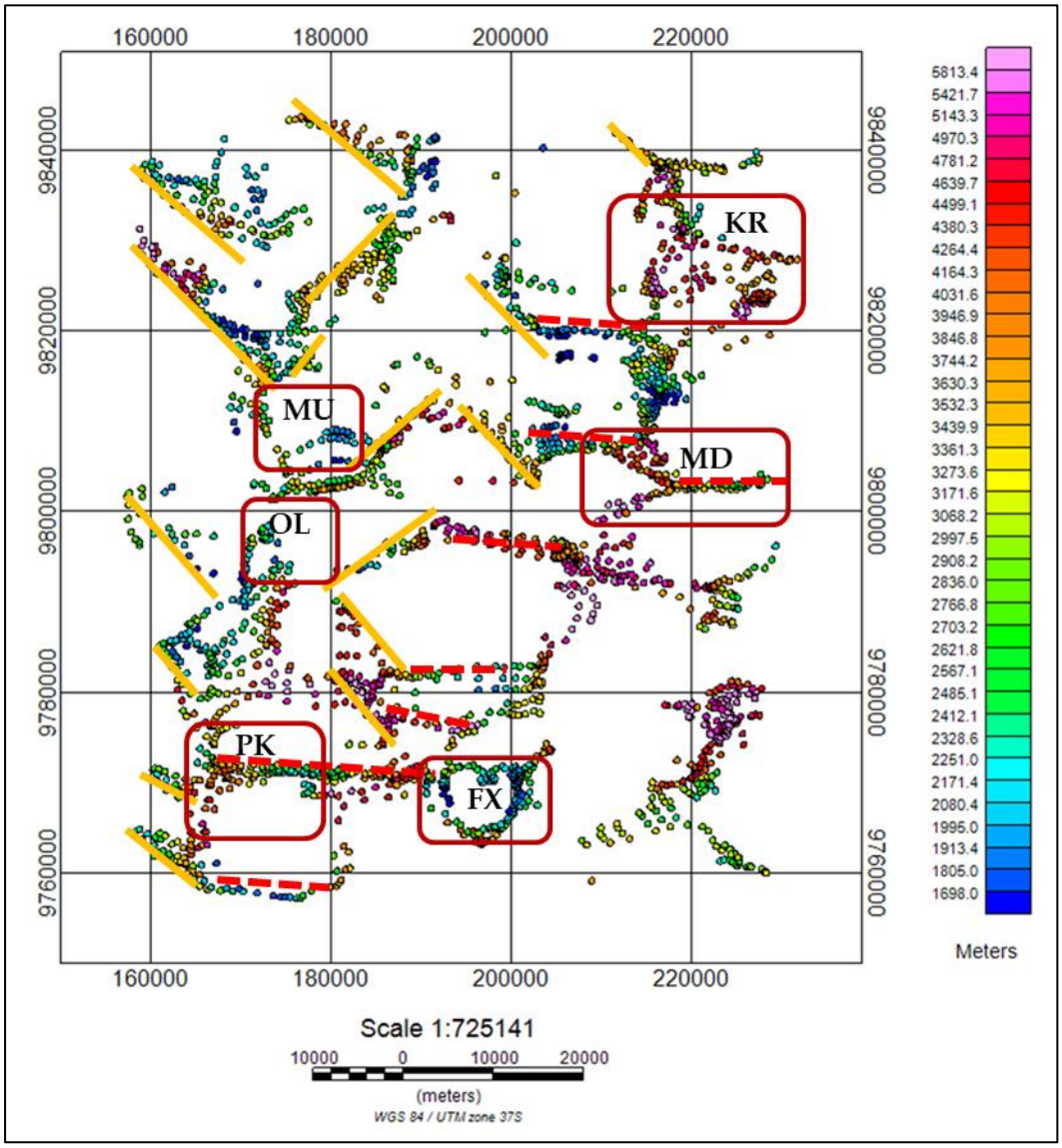

Figure 6: Euler solutions map showing the apparent depth to the causative sources

From figure 6, the clustered solutions were determined with SI = 0, a 10% margin of error, and a window size of 32km by 32km, where, KR=Koora, KD=Kordija, MD=Magadi, MU=Musenke, OK=Olkiramatian, PK=Pakase, and FX=Mile Forty-six. During the transition between Magadi and Natron, the cumulative displacement seen throughout the border fault structure remains highly fragmented. The significant decrease in displacement spanning 6700m to about 5500 m in the Nguruman area to 2400m–1800 m in the Natron area is mainly attributed to the earliest and most conspicuous Nguruman boundary fault line. The results agree with [14] who comprehensively analyzed upper crustal structures, utilizing geological, gravity, well logs, and seismic profiles.

Basement depths from geophysical estimates in the Magadi basin indicate a buried syn-rift package at least 3 km thick under the Magadi axial volcano and a package at least 1.5 km thick under the Natron axial volcano. This package is thought to be related to the initial activity of the Nguruman boundary fault [81].

Table 1: Approximate depths to the top of crucial depocenters and their estimated thickness

Compartment	Min depth[m]	Max depth[m]	Thickness[m]
Koora Depocenter [KR]	1000	3200	2200
Kordija Depocenter [KD]	1800	3200	1400
Magadi Depocenter [MD]	2100	3200	1100
Mile Forty-six Depocenter [FX]	1800	3700	1900
Pakase Depocenter [PK]	1600	4200	2600
Olkiramatian Depocenter [OL]	1800	3500	1700
Musenke Depocenter [MU]	1600	4300	2700

In the second graben [G2], the notable compartments are Magadi [MD], Kordija, and the Mile Forty-six depocenters [Fig. 4]. Magadi depocenter [MD] has a northward dip and is bounded by a volcanic host in the north and the Lenderut volcanic system in the south [Fig. 4]. A gradual change in the intensity of the magnetic residual signatures signals a relatively thinner sedimentary compartment. The residual separation results [Fig. 4] portray aeromagnetic signatures varying from -21nT to -74nT. The depth estimates made from Euler solutions [Fig. 6] and then confirmed by a 3D susceptibility model [Fig. 5] show a range of 2100 to 3200 meters, covering more than 180 square kilometers.

The Magadi depocenter [MD] is separated from the Kordija depocenter [KD] by a horst. Sedimentation in the Kordija compartment is constrained on the west by the NW-SE-oriented Kordija Fault, a manifestation of the Aswa-Nandi-Loita transfer zone [ANL] [Fig. 4]. The volcanic manifestations of the Olorgesailie platform constrain the eastern sections of the Kordija depocenters. The strength of the magnetic residual traces gradually changes, indicating comparatively thinner sedimentary strata. The findings of the residual analysis [Fig. 4] suggest that the aeromagnetic signatures exhibit a range of values from -12nT to -84nT. From the Euler

solutions [Fig. 6] that are subsequently validated by a 3D susceptibility model [Fig. 5], the depth estimations indicate a range spanning from 1800 to 3200 meters, covering an area of over 50 square kilometers.

Mile Forty-Six compartment lies on the southernmost part of the second graben [G2]. The depocenter is bounded by Lenderut volcanic manifestation in the north and Shompole in the south. A significant change in the magnitude of the magnetic residual anomalies suggests the presence of a relatively thicker sedimentary compartment. The aeromagnetic signals vary from -12nT to -437nT, covering about 300 sq. km. The measured depths obtained from Euler solutions [Fig. 6] and later confirmed by a 3D susceptibility model [Fig. 5] demonstrate a significant variation, ranging from 1800 to 3700 meters.

The third graben [G3] borders the eastern boundary fault with the Koora basin as the most significant sedimentary compartment. Koora basin dips towards the north and is bounded by the east boundary fault and the Olorgesailie volcanic system. A noticeable change in the intensity of the magnetic residual signatures indicates a comparatively thicker sedimentary compartment. Based on the magnetic residual analysis results, the variations in the aeromagnetic signatures range from -12nT to -437nT, covering an area of over 400 square kilometers. The depth estimates derived from Euler solutions [Fig. 6] and subsequently validated by a 3D susceptibility model [Fig. 5] reveal a considerable range, spanning from 1000 to 3200 meters.

Thick sedimentary sequences within the first graben imply higher chances for hydrocarbon prospecting compared to the thinner sedimentary sequences in the other two grabens.

4.3 Lineaments and structural characterization of the southern Kenya rift

The three grabens exhibit different linear structures due to the other strain regimes. A series of rotated fault blocks [T1] dominate the first graben [G1] [81]. The tilt derivative anomaly [TDR] map delineates NW-SE oriented linear structures close to the western boundary fault system [Fig. 7]. The linear anomalies are interpreted as fault lines along the rotated fault blocks. The rotated fault blocks take up the orientation of the Aswa-Nandi-Loita transfer zone [ANL] [Fig. 4b and 7]. The NW-SE-oriented faults parallel to one another are semi-parallel to the Aswa-Nandi-Loita transfer zone [ANL] [Fig. 4, 7]. A fault-bounded compartment with a northwest-southeast orientation separates the western border fault and the right-lateral strike-slip faults associated with the Aswa-Nandi-Loita transfer zone [Fig. 4, 6, and 7]. According to [81], the Aswa-Nandi-Loita [ANL] transfer zone, which is oriented in a NW-SE direction, intersects with Lower Pleistocene trachyte as well as Quaternary undifferentiated and Recent deposits. Tilt derivative findings indicate that the tilted fault block compartments [T1] have small-scale graben and horst structures [Fig. 7]. The terminations of these structures at the western boundary fault exhibit parallel or sub-parallel alignments [Fig. 4, 6, and 7].

Research conducted by [82] demonstrates that the en-echelon structures tend to form parallel to the optimum horizontal stress, which is aligned in the NE-SW direction (1/hmax), and perpendicular to the lowest horizontal stress, which is aligned in the NW-SE direction (3/hmin). The Southern Kenya Rift is partly compartmentalized by these en-echelon formations [Fig. 4, 6,

and 7]. The zigzag map architecture exhibits many fault segments, often ranging from 7 to 8, as discussed by [83]. These fault segments span a length of 1 km to 30 km which agrees [20]. The second graben [G2] lies in the axial zone [T2] characterized by E-W and NE-SW linear structures [Fig. 6, 7]. The NE-SW-oriented faults are orthogonal to the Aswa-Nandi-Loita transfer zone [ANL] [Fig. 4, 6, and 7]. The axial strip is 15 km broad and is cut into sections by an array of normal and synthetic faults that are tightly spaced (<1 km) [Fig. 6, 7]. Fault lengths in the axial compartment typically vary from 2 to 50 kilometers. Under the rift axis, receiver function modeling shows oblique regions of thinned lithosphere that are directed NE/SW [84]. The transverse rift trends identified by stress tensors, geodetic data, and investigations of earthquakes are oblique to the EW extension [85]. The transverse rift trends originated due to local stress rotations or hereditary traits [86]. An episode of flood lava effusion of the Magadi trachyte deposited on the subsiding Magadi basin (c. 400 m-thick) during the 1.3-0.9 Ma (Calabrian) [44]. Numerous normal faults parallel to the Rift fragmented the Magadi trachyte in the late rifting stage, indicating a substantial alteration [87]. Scientists have shown that magma and its associated volatile emission cause strain to migrate inward toward the rift axis [44, 47]. From a more local perspective, transverse basement structures are hypothesized to impact the architecture and movements of recent intra-rift systems in the Magadi trough's Kordija fault zone [82, 88].

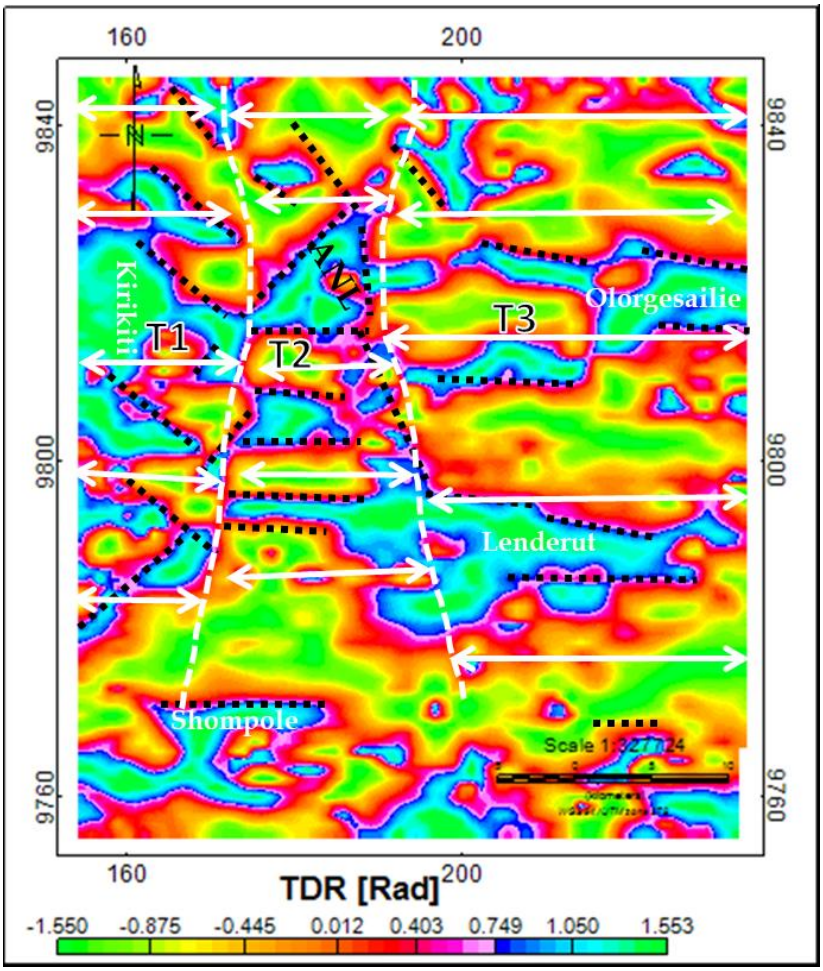

Figure 7: Tilt derivative anomaly map showing the distribution of linear structures

The third graben [G3] is interpreted as a flexural margin [T3] characterized by E-W volcano-tectonic faulting [Fig. 7], where T1= rotated fault blocks, T2= axial zone, and T3= flexural margin. The eastern flexural margin, which spans over 30 km in width, exhibits a monocline with less faulting and a consistent westward dip. This monocline is influenced by an orogenic load from the Olorgesailie, which provides a suitable area for sediment infill. The flexural side is intersected by a few extension faults that exhibit dips opposite to the western boundary fault [81].

5. Conclusion

The aim of the research was to utilize aeromagnetic and gravity data to analyze compartmentalization, sediment thickness, and structural characterization. Based on the comprehensive analysis of the compartmentalization, sediment thickness, and structural characterization of the southern Kenya Rift system from gravity and aeromagnetic analysis, several key conclusions have been drawn.

The southern Kenya Rift exhibits a complex pattern of compartmentalization, characterized by distinct faulted and segmented areas. This compartmentalization reflects variations in strain regimes across the rift system, with evidence suggesting different mechanisms of strain accommodation. The presence of tilted fault blocks, z-shaped depocenters, and en-echelon fault structures indicates a combination of strike-slip and extensional tectonic processes influencing rift evolution. Significant shifts in rifting style, observed in recent stages of rifting, indicate dynamic strain concentrations along fault systems within the Rift. The first graben (G1) displays tilted fault blocks, suggestive of strike-slip strain, particularly towards the boundary fault, with significant shifts in rifting style. The Aswa-Nandi-Loita transfer zone is crucial in compartmentalization, influencing fault structures and sedimentary deposition.

Analysis of sediment thickness within different grabens reveals significant variations within and between graben compartments. Sedimentary thickness tends to be more profound in the first graben compared to the second and third grabens. These variations likely result from localized tectonic activity, volcanic influence, and sedimentary infilling patterns constrained by fault orientations.

The rift system displays a diverse array of linear structures and fault patterns, reflecting the complex interplay of tectonic forces. Rotated fault blocks dominate the first and second grabens, while axial zones exhibit orthogonal fault orientations. Transverse rift trends and flexural margins provide valuable insights into the kinematics and evolution of the southern Kenya Rift.

The observed structural characteristics and sedimentary patterns suggest a multi-stage evolution of the southern Kenya Rift, involving interactions between magmatic activity, tectonic forces, and sedimentary processes. The shifting of strain accommodation mechanisms over time, as

evidenced by fault activity and changes in sedimentation patterns, highlights the dynamic nature of rift evolution.

Acknowledgments

We express our gratitude for the assistance and financial resources the German Academic Exchange Service (DAAD) offers.

References

[1] Baker, B., *Geology of the Magadi Area. Degree sheet 51, SW Quarter. Colony and Protectorate of Kenya. Geological Survey of Kenya*. 1958, Report.
[2] Baker, B., et al., *Sequence and geochronology of the Kenya rift volcanics.* Tectonophysics, 1971. **11**(3): p. 191-215.
[3] Baker, B., *Geology of the area south of Magadi.* Report Geological survey of Kenya, 1963. **61**.
[4] Zou, C.-N., et al., *Formation and distribution of volcanic hydrocarbon reservoirs in sedimentary basins of China.* 2008. **35**(3): p. 257-271.
[5] Reynolds, R.L., et al., *Rock magnetism, the distribution of magnetic minerals in the Earth's crust, and aeromagnetic anomalies.* 1990. **1924**: p. 24-45.
[6] Betts, P.G., D. Giles, and G.J.J.o.S.G. Lister, *Aeromagnetic patterns of half-graben and basin inversion: implications for sediment-hosted massive sulfide Pb–Zn–Ag exploration.* 2004. **26**(6-7): p. 1137-1156.
[7] Gunn, P., et al., *The basement elements of Tasmania.* 1997. **28**(2): p. 225-231.
[8] Henry, W., et al., *A seismic investigation of the Kenya Rift Valley.* 1990. **100**(1): p. 107-130.
[9] Mariita, N.O. and G.R.J.J.o.A.E.S. Keller, *An integrated geophysical study of the northern Kenya rift.* 2007. **48**(2-3): p. 80-94.
[10] Mechie, J., et al., *Crustal structure beneath the Kenya Rift from axial profile data.* Tectonophysics, 1994. **236**(1-4): p. 179-200.
[11] Mechie, J., et al., *A model for the structure, composition and evolution of the Kenya rift.* Tectonophysics, 1997. **278**(1): p. 95-119.
[12] Bosworth, W. and C.K.J.T. Morley, *Structural and stratigraphic evolution of the Anza rift, Kenya.* 1994. **236**(1-4): p. 93-115.
[13] Bosworth, W. and M.R.J.T. Strecker, *Stress field changes in the Afro-Arabian rift system during the Miocene to Recent period.* 1997. **278**(1-4): p. 47-62.
[14] Simiyu, S.M. and G.R. Keller, *Upper crustal structure in the vicinity of Lake Magadi in the Kenya Rift Valley region.* Journal of African earth sciences, 1998. **27**(3): p. 359-371.
[15] Byrne, G., et al., *Seismic structure of the upper mantle beneath the southern Kenya Rift from wide-angle data.* 1997. **278**(1-4): p. 243-260.
[16] Hollnack, D. and R.J.J.o.A.E.S. Stangl, *The seismicity related to the southern part of the Kenya Rift.* 1998. **26**(3): p. 477-495.
[17] Cohen, A., et al., *The Hominin Sites and Paleolakes Drilling Project: inferring the environmental context of human evolution from eastern African rift lake deposits.* Scientific Drilling, 2016. **21**: p. 1.
[18] Komolafe, A.A., et al., *Integrated Remote Sensing and Geophysical Investigations of the Geodynamic Activities at Lake Magadi, Southern Kenyan Rift.* International Journal of Geophysics, 2012. **2012**.
[19] Reeves, C., et al., *Geophysical evidence for a failed Jurassic rift and triple junction in Kenya.* 1987. **81**(2-3): p. 299-311.
[20] Kuria, Z., et al., *Active fault segments as potential earthquake sources: Inferences from integrated geophysical mapping of the Magadi fault system, southern Kenya Rift.* Journal of African Earth Sciences, 2010. **57**(4): p. 345-359.
[21] Reuter, H.I., A. Nelson, and A.J.I.J.o.G.I.S. Jarvis, *An evaluation of void-filling interpolation methods for SRTM data.* 2007. **21**(9): p. 983-1008.
[22] Baker, B.H. and J. Wohlenberg, *Structure and evolution of the Kenya rift valley.* Nature, 1971. **229**(5286): p. 538-42.
[23] Chorowicz, J., *The east African rift system.* Journal of African Earth Sciences, 2005. **43**(1): p. 379-410.
[24] Gregory, J.J.N., *The Structure of the Great Rift Valley.* 1924. **113**(2837): p. 388-388.
[25] Gregory, J.W., *The Rift Valleys and the Geology of East Africa*. 1923, JSTOR.
[26] Braile, L., et al., *The east African rift system.* 2006. **25**: p. 213-III.

[27] Furman, T., et al., *East African Rift System (EARS) plume structure: insights from Quaternary mafic lavas of Turkana, Kenya.* 2004. **45**(5): p. 1069-1088.
[28] Baker, B.H., *Geology of the Magadi Area: Degree Sheet 51 SW Quarter*. 1958: Survey, Min., Colony and Protectorate of Kenya.
[29] Atmaoui, N. and D. Hollnack, *Neotectonics and extension direction of the Southern Kenya Rift, Lake Magadi area.* Tectonophysics, 2003. **364**(1): p. 71-83.
[30] Baker, B., *Tectonics and volcanism of the southern Kenya Rift Valley and its influence on rift sedimentation.* Geological Society, London, Special Publications, 1986. **25**(1): p. 45-57.
[31] Renaut, R.W. and R.B. Owen, *The Kenya Rift Lakes: Modern and Ancient: Limnology and Limnogeology of Tropical Lakes in a Continental Rift*. 2023: Springer.
[32] Guth, A.L., *Evolution of the Southern Kenya Rift from Miocene to present with a focus on the Magadi area.* 2007.
[33] Smith, M. and P. Mosley, *Crustal heterogeneity and basement influence on the development of the Kenya Rift, East Africa.* Tectonics, 1993. **12**(2): p. 591-606.
[34] Schlüter, T. and C.J. Hampton, *Geology of East Africa.* 1997.
[35] Green, C., et al. *The African magnetic mapping project*. in *54th EAEG Meeting*. 1992. European Association of Geoscientists & Engineers.
[36] Sepulchre, P., et al., *Tectonic uplift and Eastern Africa aridification.* 2006. **313**(5792): p. 1419-1423.
[37] Kuria, Z.N., *Seismotectonics of active faults: Magadi fault system, Southern Kenya rift*. 2011: [Sl: sn].
[38] Keller, G.R., et al., *Seismic structure of the uppermost mantle beneath the Kenya rift.* Tectonophysics, 1994. **236**(1-4): p. 201-216.
[39] Meju, M.A. and V.J.J.o.G.R.S.E. Sakkas, *Heterogeneous crust and upper mantle across southern Kenya and the relationship to surface deformation as inferred from magnetotelluric imaging.* 2007. **112**(B4).
[40] Stern, R.J.J.A.r.o.e. and p. sciences, *Arc assembly and continental collision in the Neoproterozoic East African Orogen: implications for the consolidation of Gondwanaland.* 1994. **22**(1): p. 319-351.
[41] Shackleton, R.J.G.S., London, Special Publications, *Precambrian collision tectonics in Africa.* 1986. **19**(1): p. 329-349.
[42] Baker, B., R. Crossley, and G. Goles, *Tectonic and magmatic evolution of the southern part of the Kenya rift valley*, in *Petrology and Geochemistry of continental rifts*. 1978, Springer. p. 29-50.
[43] Baker, B. *An outline of the geology of the Kenya Rift Valley*. in *East African Rift System: UMC/UNESCO Seminar Nairobi, April 1965. IL Report on the geology and geophysics of the East A/rican Rift System*. 1965.
[44] Muirhead, J., et al., *Evolution of upper crustal faulting assisted by magmatic volatile release during early-stage continental rift development in the East African Rift.* 2016. **12**(6): p. 1670-1700.
[45] BAKER, B.H. and J.G. Mitchell, *Volcanic stratigraphy and geochronology of the Kedong–Olorgesailie area and the evolution of the South Kenya rift valley.* Journal of the Geological Society, 1976. **132**(5): p. 467-484.
[46] Baker, B., *Outline of the petrology of the Kenya rift alkaline province.* Geological Society, London, Special Publications, 1987. **30**(1): p. 293-311.
[47] Lee, H., et al., *Incipient rifting accompanied by the release of subcontinental lithospheric mantle volatiles in the Magadi and Natron basin, East Africa.* 2017. **346**: p. 118-133.
[48] Crosslev, *Structure and volcanism in the S. Kenya Rift.* Geodynamic evolution of the Afro-Arabian Rift System, 1979: p. 89-98.
[49] Cohen, A., et al., *The Hominin Sites and Paleolakes Drilling Project: inferring the environmental context of human evolution from eastern African rift lake deposits.* Sci. Dril., 2016. **21**: p. 1-16.
[50] Eugster, H., *Lake Magadi, Kenya: a model for rift valley hydrochemistry and sedimentation?* Geological Society, London, Special Publications, 1986. **25**(1): p. 177-189.
[51] Reynolds, J.M., *An introduction to applied and environmental geophysics*. 2011: John Wiley & Sons.
[52] Ravat, D.J.J.o.E. and E. Geophysics, *Analysis of the Euler method and its applicability in environmental magnetic investigations.* 1996. **1**(3): p. 229-238.
[53] Thompson, D.J.G., *EULDPH: A new technique for making computer-assisted depth estimates from magnetic data.* 1982. **47**(1): p. 31-37.
[54] Reid, A.B., et al., *Magnetic interpretation in three dimensions using Euler deconvolution.* 1990. **55**(1): p. 80-91.
[55] Corner, B., R. Durrheim, and L.J.T. Nicolaysen, *Relationships between the Vredefort structure and the Witwatersrand basin within the tectonic framework of the Kaapvaal craton as interpreted from regional gravity and aeromagnetic data.* 1990. **171**(1-4): p. 49-61.
[56] Fairhead, J., et al., *Euler: beyond the "black box"*, in *SEG Technical Program Expanded Abstracts 1994*. 1994, Society of Exploration Geophysicists. p. 422-424.

[57] Huang, D., et al. *Combined study of Euler's homogeneity equation for gravity and magnetic field*. in *57th EAGE Conference and Exhibition*. 1995. European Association of Geoscientists & Engineers.
[58] Klingele, E., I. Marson, and H.G.J.G.P. Kahle, *Automatic interpretation of gravity gradiometric data in two dimensions: vertical gradient 1.* 1991. **39**(3): p. 407-434.
[59] Marson, I. and E.J.G. Klingele, *Advantages of using the vertical gradient of gravity for 3-D interpretation.* 1993. **58**(11): p. 1588-1595.
[60] FitzGerald, D., A. Reid, and P. McInerney. *New discrimination techniques for Euler deconvolution*. in *8th SAGA Biennial Technical Meeting and Exhibition*. 2003. European Association of Geoscientists & Engineers.
[61] Gunn, P.J.J.G.p., *Linear transformations of gravity and magnetic fields.* 1975. **23**(2): p. 300-312.
[62] Zhang, C., et al., *Euler deconvolution of gravity tensor gradient data.* 2000. **65**(2): p. 512-520.
[63] Miller, H.G. and V.J.J.o.a.G. Singh, *Potential field tilt—a new concept for location of potential field sources.* 1994. **32**(2-3): p. 213-217.
[64] Verduzco, B., et al., *New insights into magnetic derivatives for structural mapping.* The Leading Edge, 2004. **23**(2): p. 116-119.
[65] Salem, A., et al., *Interpretation of magnetic data using tilt-angle derivatives.* 2008. **73**(1): p. L1-L10.
[66] Ansari, A. and K. Alamdar, *A new edge detection method based on the analytic signal of tilt angle (ASTA) for magnetic and gravity anomalies.* 2011.
[67] Blakely, R.J. and R.W.J.G. Simpson, *Approximating edges of source bodies from magnetic or gravity anomalies.* 1986. **51**(7): p. 1494-1498.
[68] Fedi, M. and M.J.G. Pilkington, *Understanding imaging methods for potential field data.* 2012. **77**(1): p. G13-G24.
[69] Oruç, B.J.J.o.A.G., *Location and depth estimation of point-dipole and line of dipoles using analytic signals of the magnetic gradient tensor and magnitude of vector components.* 2010. **70**(1): p. 27-37.
[70] Phillips, J.D., R.O. Hansen, and R.J.J.E.G. Blakely, *The use of curvature in potential-field interpretation.* 2007. **38**(2): p. 111-119.
[71] Wijns, C., C. Perez, and P.J.G. Kowalczyk, *Theta map: Edge detection in magnetic data.* 2005. **70**(4): p. L39-L43.
[72] Ingram, D.M., et al., *Developments in Cartesian cut cell methods.* 2003. **61**(3-6): p. 561-572.
[73] Ellis, R. and I.J.A.E.A. MacLeod, *Constrained voxel inversion using the Cartesian cut cell method.* 2013. **2013**(1): p. 1-4.
[74] Roy, R., et al., *Three-dimensional gravity modelling applied to the exploration of uranium unconformity-related basement-hosted deposits: the Contact prospect case study, Kiggavik, northeast Thelon region (Nunavut, Canada).* 2017. **54**(8): p. 869-882.
[75] Barbosa, R.D. and J.G. Pereira. *Inversão 3D de dados Magnéticos na Região de Mara Rosa-Goiás, Brasil, utilizando Geosoft VOXI*. in *13th International Congress of the Brazilian Geophysical Society & EXPOGEF, Rio de Janeiro, Brazil, 26–29 August 2013*. 2013. Society of Exploration Geophysicists and Brazilian Geophysical Society.
[76] Farhi, W., et al., *Integration of magnetic, gravity, and well data in imaging subsurface geology in the Ksar Hirane region (Laghouat, Algeria).* 2016. **124**: p. 63-74.
[77] Bhattacharyya, B.J.G., *Two-dimensional harmonic analysis as a tool for magnetic interpretation.* 1965. **30**(5): p. 829-857.
[78] Dampney, C.J.G., *The equivalent source technique.* 1969. **34**(1): p. 39-53.
[79] Dransfield, M. and B. Milkereit. *Airborne gravity gradiometry in the search for mineral deposits*. in *Proceedings of exploration*. 2007.
[80] Pedersen, L.B. and T.M.J.G. Rasmussen, *The gradient tensor of potential field anomalies; some implications on data collection and data processing of maps.* 1990. **55**(12): p. 1558-1566.
[81] Le Gall, B., et al., *The anomalously-propagating South Kenya rift in the context of the North Tanzanian Divergence zone, East Africa.* 2021. **814**: p. 228968.
[82] Le Turdu, C., et al., *Influence of preexisting oblique discontinuities on the geometry and evolution of extensional fault patterns: evidence from the Kenya Rift using SPOT imagery.* Geoscience of Rift Systems–Evolution of East Africa, 1999. **44**: p. 173-91.
[83] Vétel, W., B. Le Gall, and J.J.J.J.o.S.G. Walsh, *Geometry and growth of an inner rift fault pattern: the Kino Sogo Fault Belt, Turkana Rift (North Kenya).* 2005. **27**(12): p. 2204-2222.
[84] Plasman, M., et al., *Lithospheric low-velocity zones associated with a magmatic segment of the Tanzanian Rift, East Africa.* 2017. **210**(1): p. 465-481.
[85] Ibs-von Seht, M., et al., *Seismicity, seismotectonics and crustal structure of the southern Kenya Rift—new data from the Lake Magadi area.* Geophysical Journal International, 2001. **146**(2): p. 439-453.

[86] Weinstein, A., et al., *Fault-magma interactions during early continental rifting: Seismicity of the M agadi-N atron-M anyara basins, A frica.* 2017. **18**(10): p. 3662-3686.
[87] Baker, B., J.G. Mitchell, and L.J.J.o.t.G.S. Williams, *Stratigraphy, geochronology and volcano-tectonic evolution of the Kedong–Naivasha–Kinangop region, Gregory Rift Valley, Kenya.* 1988. **145**(1): p. 107-116.
[88] Muirhead, J. and S.J.J.o.S.G. Kattenhorn, *Activation of preexisting transverse structures in an evolving magmatic rift in East Africa.* 2018. **106**: p. 1-18.